ADVANCED MATERIALS TECHNOLOGIES
www.advmattechnol.de

Thermoelectric Paper: Graphite Pencil Traces on Paper to Fabricate a Thermoelectric Generator

*Rafiq Mulla, Daniel R. Jones, and Charles W. Dunnill**

Paper-based thermoelectric generators are a promising and economical alternative to expensive organic conductors that are normally preferred for flexible generators. In the present work, graphite pencil traces on regular Xerox paper are successfully employed to constitute a thermoelectric generator. In conjunction with polyethylenimine polymer, the graphite traces act as both the p-type and n-type thermoelectric "legs," of a graphite-based thermoelectric generator. The fabrication method is facile and requires no conducting paste or silver paste to connect individual thermoelectric legs. A test module containing five pairs of p-n legs is fabricated on paper to test its performance. The device produces a thermoelectric voltage of 9.2 mV, generating an output power of 1.75 nW at a temperature difference of ≈60 K. The present work demonstrates that ordinary pencil on paper may be used as the foundation for a cheap, flexible, easily disposable, and environmentally friendly thermoelectric generator.

1. Introduction

Thermoelectric generators can generate electricity under temperature gradients, or vice versa, and therefore they provide a pollution-free method to produce useful electric power from waste heat or solar radiation.[1] Employing thermoelectric generators to power electrolysis allows hydrogen to be produced from these renewable sources, thereby providing a means of storing the energy in order to circumvent intermittency of the available supply.[1b,2] At present, commercial thermoelectric generators are mainly based on elements such as Bi, Te, and Pb, but issues such as the high cost, scarcity, and toxicity of these elements have inhibited progress of the technology.[3]

In order to overcome the problems associated with traditional thermoelectric materials, researchers have begun to focus on more sustainable and inexpensive alternatives such as metal sulfides, oxides, carbon-based composites, and organic/polymer compounds.[3b,4] Among the materials under investigation, several carbon-based compounds offer notable promise due to their characteristically low-cost, nontoxicity, and competitive electrical properties.[5] Graphite, an allotrope of carbon naturally available in the form of different minerals, is abundant, environmentally friendly therefore, can be advantageous if employed in energy-related applications and it can also be used for thermoelectric applications by creating porous or foam-like composites which helps reduce thermal conductivity.[6] Recently, carbon nanotubes (CNT's) have been studied extensively for thermoelectric applications, with most of the studies focused on flexible devices based on CNT/polymer composites.[7] An important aspect to note is that the making of flexible devices often relies on organic conductors such as poly(3,4-ethylenedioxythiophene)/poly(styrenesulfonate), popularly known as PEDOT/PSS, and other related organic/polymers that offer limited scalability due to their high cost.[8] Likewise, many inorganic thermoelectric powders, which often contain hazardous and expensive materials such as tellurium,[9] metal tellurides,[10] and selenides,[11] are typically mixed with polymers or organic compounds to obtain flexible and free-standing thermoelectric devices. Conversely, a couple of studies have promoted paper as a flexible substrate for electronic devices.[6a,10g,12] Pencil on paper has been studied as a material for sensors,[13] energy storage devices,[14] and electronic circuits,[15] among other applications. Very recently, pencil/InSe traces have been used as n-type legs for thermoelectric applications in conjunction with p-type PEDOT/PSS legs.[8e] The present work expands on this concept by developing pencil traces on a paper that function as both p-type and n-type legs, thereby facilitating the production of a graphite-only thermoelectric generator.

2. Results and Discussion

The pencil- and paper-based thermoelectric device fabrication process is schematically shown by **Figure 1**, and the real pictures of the generator are shown in **Figure 2**. The properties of individual p-type and n-type graphite traces (Trace Design 1 (TD1)) were studied before analyzing the performance of the device (Trace Design 2 (TD2)) which are discussed in the following sections.

Dr. R. Mulla, Dr. D. R. Jones, Dr. C. W. Dunnill
Energy Safety Research Institute
Swansea University
Bay Campus, Fabian Way, Swansea SA1 8EN, UK
E-mail: c.dunnill@swansea.ac.uk

The ORCID identification number(s) for the author(s) of this article can be found under https://doi.org/10.1002/admt.202000227.

DOI: 10.1002/admt.202000227

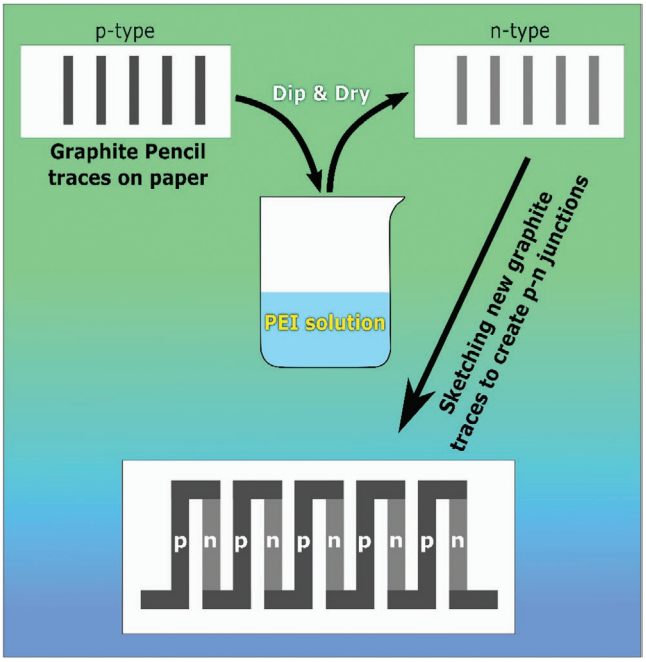

Figure 1. A Schematic illustration showing the fabrication steps of a 5-pair TD2 thermoelectric generator on Xerox paper.

2.1. Thermoelectric Properties of the TD1 Sample

The room temperature Seebeck coefficient of an as-drawn TD1 sample was +16.1 μV K^{-1}, where the positive value is consistent with p-type electrical conductivity; as shown in **Figure 3**a, increasing the temperature up to 100 °C had a negligible effect on this value. Following PEI-treatment of the graphite trace, however, the room temperature Seebeck coefficient changed to a negative value of −21.5 μV K^{-1}, which is indicative of the successful conversion from p- to n-type behaviour. Furthermore, it is evident from Figure 3b that the Seebeck coefficient of the PEI-treated trace exhibited a small but significant variation with respect to temperature, increasing in magnitude to a value of −23.2 μV K^{-1} at 100 °C.

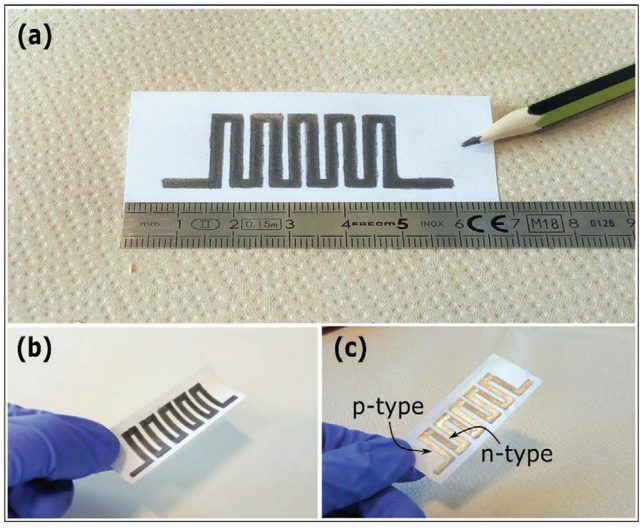

Figure 2. a,b) Photographs of a TD2 thermoelectric generator; the scale of the device is evident from images. c) Visual differences between the p-type and n-type legs can be observed in photograph.

Alongside the Seebeck coefficient, the electrical conductivity and power factor of a thermoelectric material are critical to its overall performance as part of a device; these measurements are plotted from room temperature to 100 °C for the as-drawn and PEI-treated TD1 devices in Figure 3c,d, respectively. Despite the considerable increase in resistivity yielded by PEI-treatment, with the room temperature conductivity decreasing from 3.32×10^2 S m^{-1} for as-drawn graphite to 2.24×10^2 S m^{-1}, the power factor was correspondingly improved by the treatment process: the measured value of 85 nW m^{-1} K^{-2} in the case of untreated graphite was increased to 100 nW m^{-1} K^{-2} after modification by PEI. Moreover, increasing the temperature resulted in a still greater difference between the power factors of the two samples, as shown by Figure 3d.The strategy of changing conductivity type of a pencil trace was inspired by earlier reports where researchers have changed the behaviour of CNT's from p-type to n-type by using PEI and other polymers.[16]

Reproducibility of the thermoelectric properties is also an important aspect of generator design. To test, measurements have been repeated 2–3 times on the pencil trace to ensure the reproducibility in the values and observed stable values over repeated measurements. It was also noted that there were small deviations in the Seebeck values from one sample to another but this change was found to be less than ± 3 μV K^{-1}.

The thermoelectric figure of merit (ZT) of the as-drawn and PEI-treated graphite traces have been estimated using the standard expression, $ZT = S^2\sigma T/\kappa$, where S, σ, κ, and T are the Seebeck coefficient, electrical conductivity, thermal conductivity, and temperature respectively. Thermal conductivity value (in-plane, κ= 3.5 W m^{-1} K^{-1} at 100 °C) has been obtained from the literature on reduced graphene oxide films having similar electrical conductivity.[17] The estimated ZT values of the as-drawn and PEI-treated graphite trace at 100 °C are 1.01×10^{-5} and 1.32×10^{-5} respectively, which are very low in contrast to widespread thermoelectric materials but comparable to previous reports.[17,18]

A key advantage of employing paper as a foundation for thermoelectric devices is its flexibility, as pictured in **Figure 4**. However, in order for an application to exploit this property over the long-term, it is necessary for the device to demonstrate sustainable performance through multiple cycles of distortion. To this end, changes in the Seebeck coefficient and electrical conductivity of a TD1 sample were measured over multiple bending cycles, as depicted in **Figure 5**a; separate but identical TD1 type samples were used for the Seebeck coefficient and electrical conductivity measurements, which are plotted in Figure 5b,c, respectively. The electrical conductivity decreased by ≈2.2% over 600 bending cycles, although there was concurrently negligible variation in the Seebeck coefficient within the experimental errors. The small decrease in electrical conductivity may be attributed to the formation of fractures between graphite structures during the cyclical bending process; nevertheless, the durability of the graphite-based thermoelectric generator is demonstrated by the low magnitude of this conductivity variation, despite the substantial and repeated distortion applied to the device. Further, the Seebeck coefficients of the TD1 type samples were measured under different bending conditions

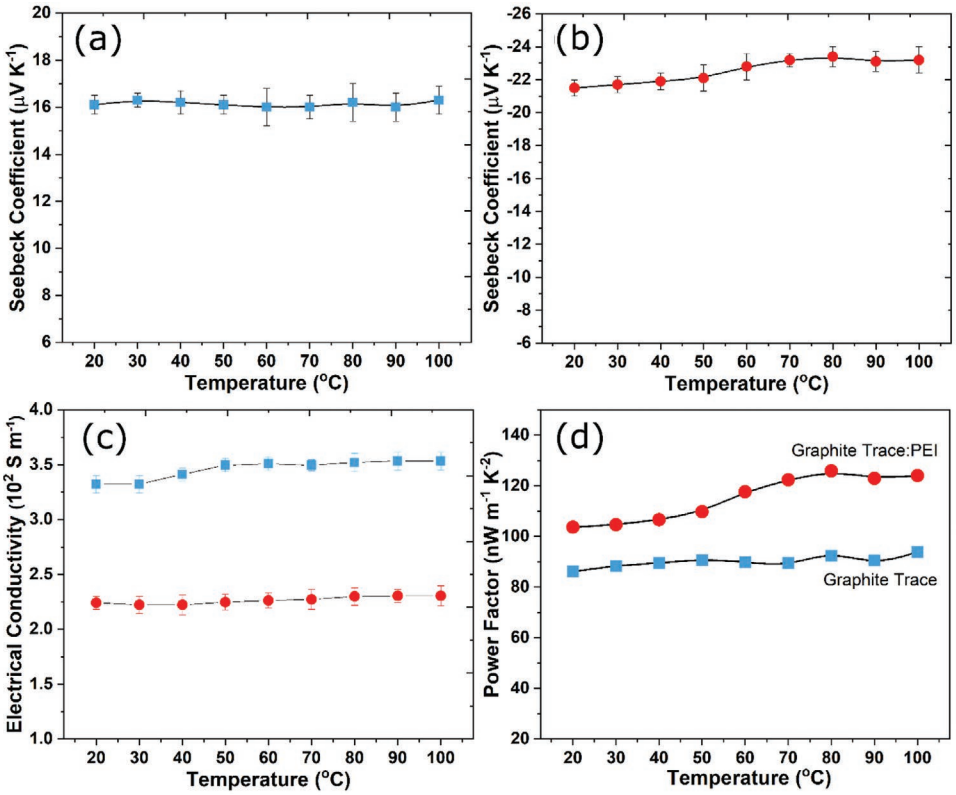

Figure 3. Measured variations of the Seebeck coefficient of a) as-drawn graphite and b) PEI-treated graphite in the TD1 configuration, in addition to the corresponding changes in c) electrical conductivity and d) power factor of the two samples.

(≈45° and ≈90°) and it was observed that the values were not much affected but a slight change of about 1 μV K^{-1} (Figure S1, Supporting Information).

2.2. Characterization of the Graphite Trace on Paper

In order to characterise the surface morphology of the graphite trace, SEM was employed; alongside an optical image of the underlying Xerox paper in **Figure 6**a, an SEM micrograph of the paper in Figure 6b is accompanied by corresponding images of as-drawn graphite trace in Figure 6c,d and a PEI-treated trace in Figure 6e,f. It is clear from the images that the porous arrangement of cellulose paper fibres was completely covered by each graphite trace, and moreover there are no significant visible differences between the layered graphite structures of as-drawn and PEI-treated samples. SEM images of higher-magnification that show thick graphitic flakes/layers can be seen in Figure S2 (Supporting Information). From the cross-sectional SEM image pictured in Figure S3 in the Supporting Information, an estimate of 3.20 (±0.05) μm is obtained for the thickness of an as-drawn graphite trace.

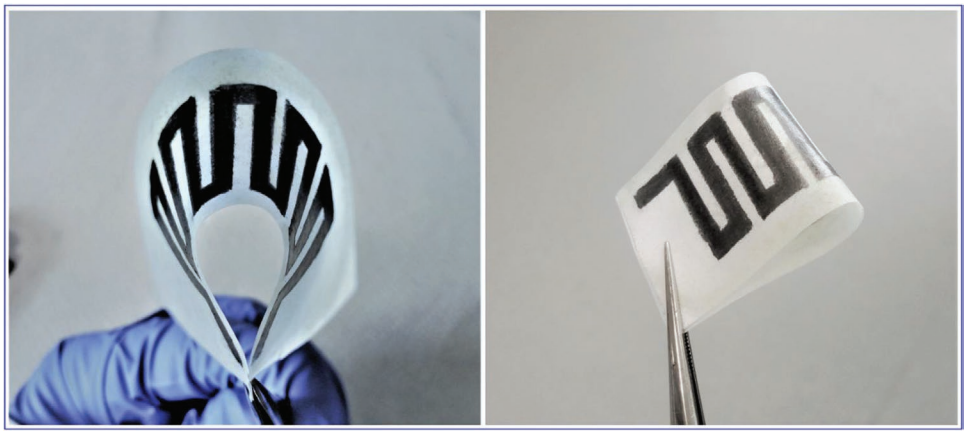

Figure 4. Photographs showing of the flexible nature of the TD2 thermoelectric generator.

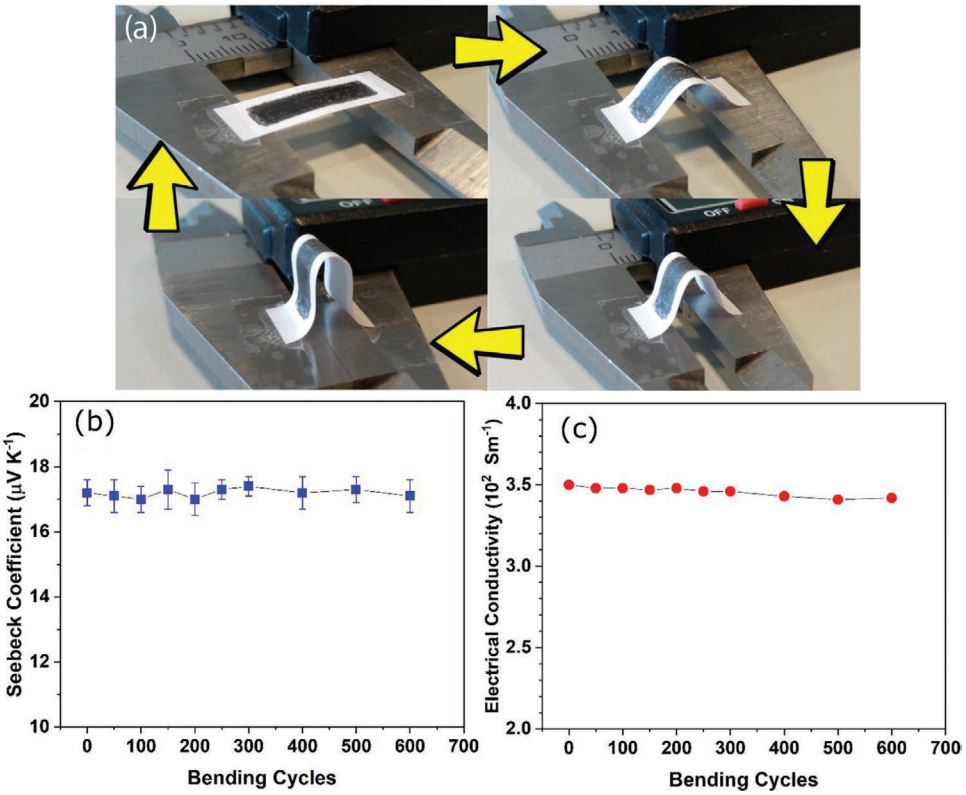

Figure 5. Photographs depicting the cyclical bending procedure applied to the a) TD1 thermoelectric trace, alongside the measured variations of the b) Seebeck coefficient and c) electrical conductivity over multiple bending cycles.

The chemical surface compositions of as-drawn and PEI-treated pencil traces were analyzed using XPS; survey spectra of these materials are shown in **Figure 7**, while higher resolution C1s spectra are displayed in **Figure 8**a,b, respectively, alongside the corresponding N1s spectrum of PEI-treated graphite in Figure 8c. The clear appearance of the N peak in the survey spectrum of PEI-treated graphite confirms the incorporation of PEI at the sample surface, while the presence of C—N chemical environments is further evident from the large component at 286.3 eV in the C1s spectrum of PEI-treated trace. From the corresponding N1s spectrum depicted in Figure 8c it is apparent that the majority of the N atoms were contained within the amine groups of PEI and pyrrolic environments at the graphite surface, with relatively little substitution of C atoms for N within the surface graphite lattice. Indeed, deconvolution of the C1s spectra also indicates that the composition of the graphite lattice was not altered significantly by the PEI-treatment: despite the emergence of C—N chemical environments, the intensity ratio of the component associated with sp^2 carbon atoms, at 284.4 eV,[19] and the other surface environments did not vary appreciably between the two samples. Alongside the C—N groups identified in Figure 8b and the sp^2 environments of both spectra, a common component at 284.8 eV can be assigned to C atoms connected in an sp^3 configuration,[20] while peaks at 286.1 and 287.2 eV are characteristic of the C atoms in ether, alcohol or carbonyl groups.[20c,21] As shown in the figure, the N1s peak can be split into two peaks with a major peak centred at 400.0 eV and a minor peak at 401.4 eV. It is normally proposed that the three predominant bonding configurations are pyridinic N, pyrrolic N, and graphitic N when nitrogen is doped into graphene or graphite.[22] In the present case, the main peak at 400.0 eV can be assigned to pyrrolic N bonding and the small peak of 401.4 eV to the graphitic N bonding.[23] It is well studied that the conversion of p-to-n-type conductivity is due to the electron-donating capability of PEI polymer through the amine groups.[24] The n-type doping is more favourable in case of PEI polymer as it contains a high density of amine groups compared to other polymers.[24]

2.3. Performance of the Thermoelectric Generator

Through use of the experimental arrangement pictured in **Figure 9**, voltage, current and power outputs were measured as a function of temperature gradient for a TD2 configuration of p- and n-type legs, as plotted in **Figure 10**. Figure 10a shows that the thermoelectric generator produced a linearly varying potential of 0.15 mV K^{-1} for a temperature gradient ΔT of up to 60 K, indicating that the Seebeck coefficient remained approximately constant over this ΔT range. Correspondingly, the estimated power outputs of the generator along with respective voltage outputs are plotted in Figure 10b. The variation of resistance at different temperature gradients with respective power outputs can be seen in Figure S4 (Supporting Information). The power generated by the generator under ≈60 K gradient was 1.75 nW.

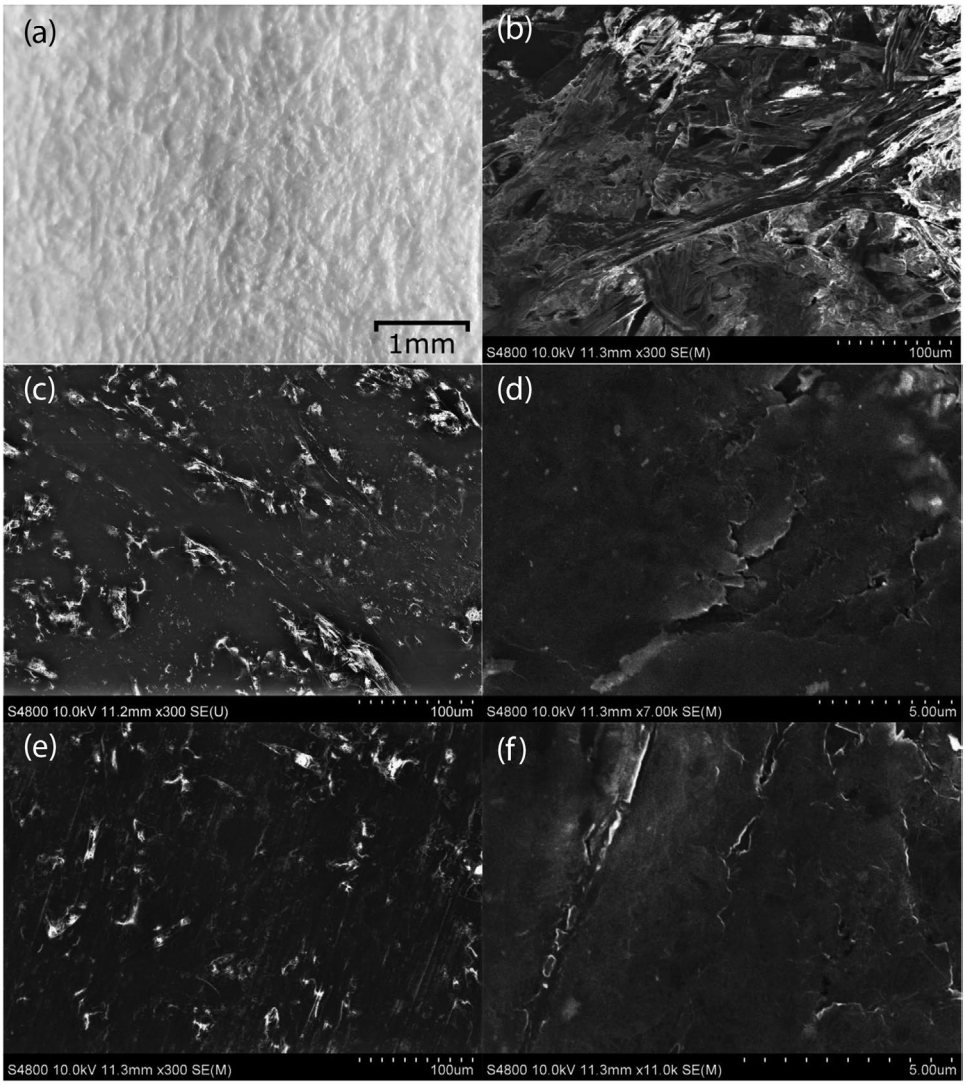

Figure 6. a) Optical microscope and SEM images showing the morphology of b) Xerox paper, c,d) an as-drawn graphite trace, and e,f) a PEI-treated graphite trace.

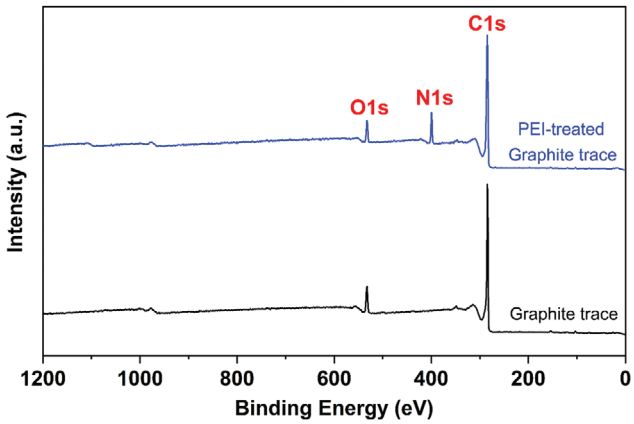

Figure 7. XPS survey spectra of as-drawn and PEI-treated pencil traces on paper.

The power produced by the generator is comparable to the power output of alternative flexible devices reported previously in the literature, but offers particular advantages with respect to the overall device size and ease of fabrication. For example, the power output is consistent with values obtained from a reduced graphene oxide (rGO) device, which yielded 1.36 nW for a 50 K temperature gradient, but one should note that this arrangement required 24 pairs of p-n legs, in contrast to the five pairs utilised in the present work.[25] The generated power is also of similar magnitude to alternative systems of far greater cost and complexity; for instance, one pair of p-n legs composed of chemically exfoliated WS_2 (n-type) and $NbSe_2$ (p-type) nanosheets produced 0.63 nW from a temperature gradient of 60 K, which extrapolates to 3.15 nW in the case of a five-leg module.[26] Similarly, a configuration containing 4.5 $Bi_2Te_3/Bi_{0.5}Sb_{1.5}Te_3$ p-n pairs produced a power of ≈6.5 nW for a ΔT value of 60 K,[27] while 4.5 p-n legs of a Bi_2Te_3/GeTe

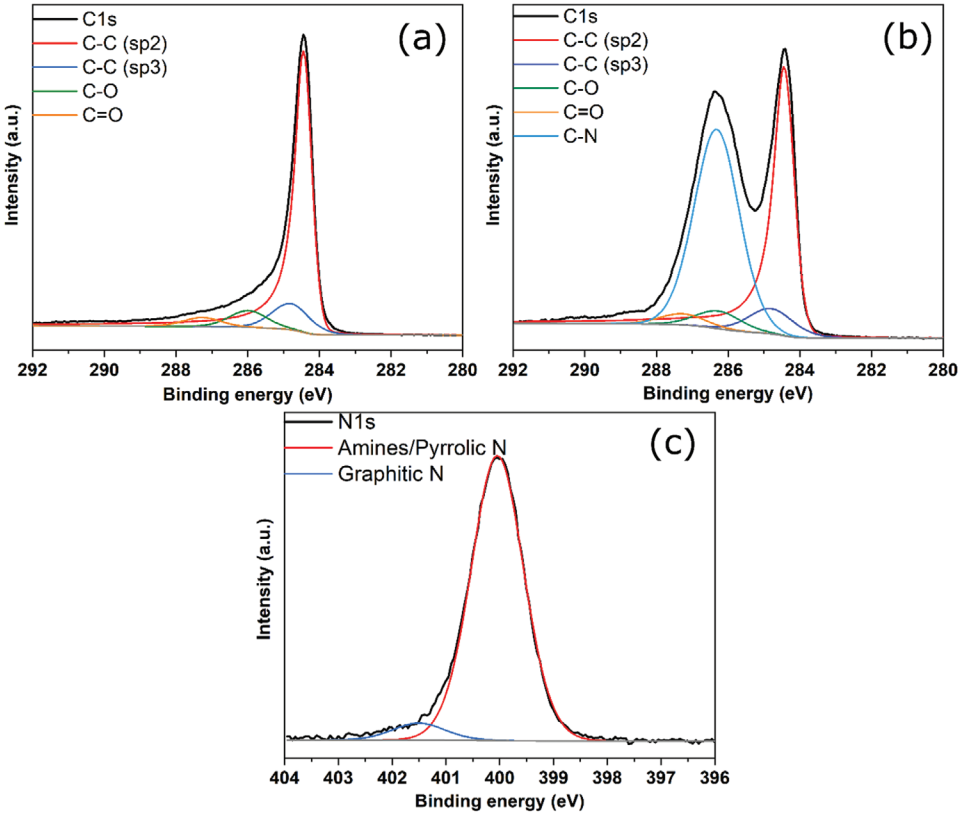

Figure 8. C1s XPS spectra of an as-drawn graphite trace on a) paper , in addition to the b) corresponding C1s and c) N1s spectra of PEI-treated graphite.

device yielded 16 nW under application of the same temperature gradient;[27] these reported values are included in **Table 1**. While these values are superior to the power output achieved in the present case, the materials and fabrication procedures utilised in these studies are notably more expensive than those employed herein.

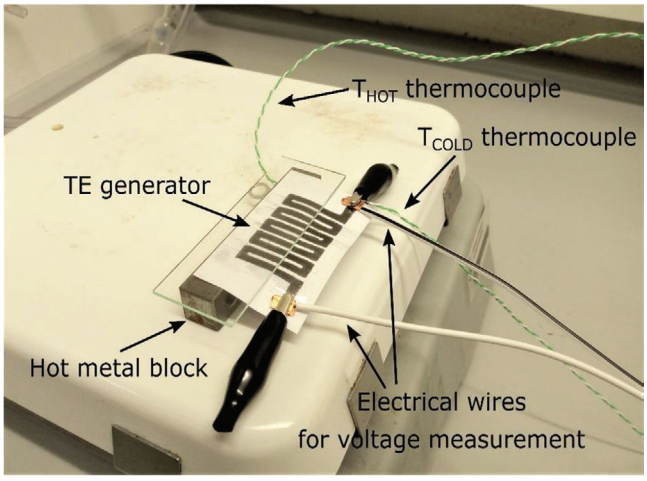

Figure 9. Photograph showing the setup used for electrical testing of the TD2 thermoelectric generator module.

3. Conclusion

The present study demonstrates a facile and novel approach to produce thermoelectric generators using ordinary pencil traces on Xerox paper, wherein it has been shown that graphitic p-n junctions may be reliably achieved via a rudimentary treatment of the graphite trace with PEI polymer. Although nature of the protocol is simple and low-cost, the power output generated by the thermoelectric generator module comprised of five graphitic p-n pairs is low. Further improvements are possible by tuning the electronic properties of the starting graphite material either by alloying or doping with other elements or compounds.

4. Experimental Section

Thermoelectric Generator Fabrication: Commonly available HB grade graphite pencil and office Xerox paper (80 g m^{-2}) were obtained from a local stationery supplier, while polyethyleneimine (PEI, branched M.W. 600) and ethanol were purchased from Alfa Aesar; all of these materials were used without any further purification. As a foundation for the thermoelectric generators, graphite traces were drawn by hand onto Xerox paper, with multiple layers applied in order to achieve high connectivity between the graphitic structures. To alter the majority charge carriers in the graphite traces and thereby transform the material from p-type to n-type, they were treated with a solution of PEI (2 mL) in ethanol (20 mL); this volumetric ratio was selected following an optimisation procedure outlined in the Supporting Information, wherein Figure S5 in the Supporting Information compares various electrical

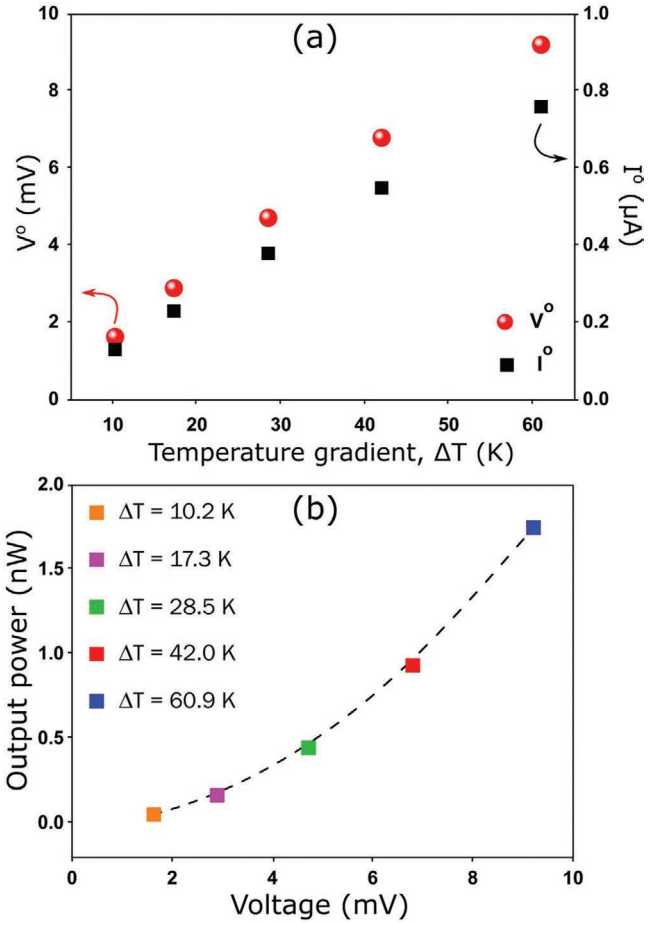

Figure 10. The open circuit voltage (V^o) and short circuit current (I^o) generated by the five p-n legs of a TD2 thermoelectric generator plotted as a function of a) temperature gradient ΔT, as well as b) the corresponding power output ($V^oI^o/4$) versus voltage with respect to ΔT.

characteristics of graphite traces treated with different ethanolic PEI solutions. In particular, traces immersed in the chosen ethanolic PEI solution exhibited a higher thermoelectric power factor than counterparts treated with solutions of alternative composition. The traces were immersed in solution for 4 h and then dried overnight at 70 °C under open-air conditions. Excess polymer coating was removed by subsequently rinsing the traces in absolute ethanol, before drying in air under ambient conditions. During the investigations, two trace designs were employed:

Trace Design 1 (TD1): For initial measurements of the Seebeck coefficient and characterization of the material morphology and surface chemistry, a rectangular trace of length 15 mm and width 5 mm was used.

Trace Design 2 (TD2): Optimisation of thermoelectric devices containing multiple p-n junctions was achieved using a track in the form of a "square wave," as illustrated in Figure 1 alongside a schematic of the PEI immersion step. The n-type section of this design was composed of five rectangular graphite traces, or "legs," of approximate width 2 mm and length 15 mm, with a separation of ≈6 mm between legs. In order to ensure homogeneity within the design, the resistance along the length of each leg was measured and approximately equal resistance was achieved in all cases. After immersing this design in ethanolic PEI solution to achieve n-type characteristics, the five legs were connected by five parallel and uniformly spaced p-type graphite legs of identical length and width. The completed form of TD2 is shown in Figure 2, which displays photographs of the completed thermoelectric module; notably, it is evident from the image in Figure 2c that the p-type and n-type legs could be distinguished from a marked difference in their reflective properties, with the n-type legs appearing distinctively duller than the adjoining p-type traces.

Thermoelectric Testing: The as-drawn TD1 sample was cut from the paper and the Seebeck coefficient was measured by applying a temperature gradient along its length using a home-built apparatus.[10e] The electrical conductivity of the trace was measured using the standard four-probe method.

Current and potential measurements were carried out using HMC 8012 DMM digital multimeters and regulated power supply. The thermoelectric performance of the TD2 generator was tested by applying different temperature gradients by mounting it on a hot plate.

Material Characterization: The as-drawn and PEI-treated graphite traces were examined by scanning electron microscopy (SEM) using Hitachi S4800 FE-SEM system and X-ray photoelectron spectroscopy (XPS) using Kratos Axis Supra system having a monochromatic Al-Kα X-ray source. For XPS scanning, samples of pencil trace on paper (5 mm x 5 mm) were mounted on copper tape. To achieve electrical contact between the pencil trace and the stage, copper clips were screwed in; the XPS scanning's were performed over an area of 700 × 300 µm. Survey scanning was performed across energy range of 0–1200 eV at a step size 1 eV using pass energy 160 eV and dwell time 100 ms. Core level spectra were recorded using pass energy 20 eV, dwell time 1000 ms, with a step size 50 meV. Charge compensation was achieved with a charge neutralizer working at a potential of 3.3 V with filament bias of 1.0 V and filament current of 0.4 A. All the measured data of the core level scanning were fitted with Gaussian–Lorentzian components.

Table 1. Power output comparison of the pencil- and paper-based generator with other reported devices.

Device details	Number of p-n junctions	Temperature gradient [K]	Power output [nW]	Reference
Pencil traces/PEI treated pencil traces on paper	5	60	1.75	This work
n-InSe:graphite/PEDOT:PSS on paper	1	50	10	[8e]
rGO/PEI-doped rGO films	24	50	1.36	[25]
$WS_2/NbSe_2$ nanosheets	1	60	0.63	[26]
$WS_2/NbSe_2$ nanosheets	100	60	38	[26]
$Bi_2Te_3/Bi_{0.5}Sb_{1.5}Te_3$ thin films	4.5	60	6.5	[27]
Bi_2Te_3/GeTe thin films	4.5	60	16	[27]

Supporting Information

Supporting Information is available from the Wiley Online Library or from the author.

Acknowledgements

The authors are thankful to the Welsh Government (EU European Regional Development Fund) for funding the RICE (Reducing Industrial Carbon Emission) project (Grant Number: 81435).

Conflict of Interest

The authors declare no conflict of interest.

Keywords

graphite, paper generator, pencil art, thermoelectric generators

Received: March 16, 2020
Revised: April 13, 2020
Published online:

[1] a) J. He, T. M. Tritt, *Science* **2017**, *357*, eaak9997; b) R. Mulla, C. W. Dunnill, *ChemSusChem* **2019**, *12*, 3882.

[2] a) D. R. Jones, W. A. Al-Masry, C. W. Dunnill, *Sustainable Energy Fuels* **2018**, *2*, 710; b) R. Phillips, C. W. Dunnill, *RSC Adv.* **2016**, *6*, 100643; c) R. Phillips, A. Edwards, B. Rome, D. R. Jones, C. W. Dunnill, *Int. J. Hydrogen Energy* **2017**, *42*, 23986.

[3] a) A. K. Bohra, R. Bhatt, A. Singh, R. Basu, S. Bhattacharya, K. N. Meshram, S. Ahmad, A. K. Debnath, A. K. Chauhan, P. Bhatt, K. Shah, K. Bhotkar, S. Sharma, D. K. Aswal, K. P. Muthe, S. C. Gadkari, *Energy Convers. Manage.* **2017**, *145*, 415; b) R. Mulla, M. H. K. Rabinal, *Energy Technol.* **2019**, *7*, 1800850.

[4] a) G. Dennler, R. Chmielowski, S. Jacob, F. Capet, P. Roussel, S. Zastrow, K. Nielsch, I. Opahle, G. K. H. Madsen, *Adv. Energy Mater.* **2014**, *4*, 1301581; b) Z.-H. Ge, L.-D. Zhao, D. Wu, X. Liu, B.-P. Zhang, J.-F. Li, J. He, *Mater. Today* **2016**, *19*, 227; c) M. R. Burton, S. Mehraban, J. McGettrick, T. Watson, N. P. Lavery, M. J. Carnie, *J. Mater. Chem. A* **2019**, *7*, 25586; d) R. Mulla, M. K. Rabinal, *Ultrason. Sonochem.* **2017**, *39*, 528; e) X. Crispin, *Nat. Energy* **2016**, *1*, 16037.

[5] a) Y. Anno, Y. Imakita, K. Takei, S. Akita, T. Arie, *2D Mater.* **2017**, *4*, 025019; b) T. G. Novak, J. Kim, J. Kim, H. Shin, A. P. Tiwari, J. Y. Song, S. Jeon, *2D Mater.* **2019**, *6*, 045019; c) M.-H. Lee, Y. H. Kang, J. Kim, Y. K. Lee, S. Y. Cho, *Adv. Energy Mater.* **2019**, *9*, 1900914.

[6] a) N. Kurra, G. U. Kulkarni, *Lab Chip* **2013**, *13*, 2866; b) D. Olaya, M. Hurtado-Morales, D. Gómez, O. A. Castañeda-Uribe, Z.-Y. Juang, Y. Hernández, *2D Mater.* **2017**, *5*, 011004; c) R. Mulla, C. W. Dunnill, *Compos. Commun.* **2020**, https://doi.org/10.1016/j.coco.2020.04.011.

[7] a) G. Wu, C. Gao, G. Chen, X. Wang, H. Wang, *J. Mater. Chem. A* **2016**, *4*, 14187; b) K. Yusupov, S. Stumpf, S. You, A. Bogach, P. M. Martinez, A. Zakhidov, U. S. Schubert, V. Khovaylo, A. Vomiero, *Adv. Funct. Mater.* **2018**, *28*, 1801246; c) C. T. Hong, Y. H. Kang, J. Ryu, S. Y. Cho, K.-S. Jang, *J. Mater. Chem. A* **2015**, *3*, 21428.

[8] a) Q. Wei, M. Mukaida, K. Kirihara, T. Ishida, *ACS Macro Lett.* **2014**, *3*, 948; b) D. A. Mengistie, C.-H. Chen, K. M. Boopathi, F. W. Pranoto, L.-J. Li, C.-W. Chu, *ACS Appl. Mater. Interfaces* **2015**, *7*, 94; c) Y. Du, J. Xu, B. Paul, P. Eklund, *Appl. Mater. Today* **2018**, *12*, 366; d) S. H. Lee, H. Park, S. Kim, W. Son, I. W. Cheong, J. H. Kim, *J. Mater. Chem. A* **2014**, *2*, 7288; e) V. V. Brus, M. Gluba, J. Rappich, F. Lang, P. D. Maryanchuk, N. H. Nickel, *ACS Appl. Mater. Interfaces* **2018**, *10*, 4737; f) L. K. Allison, T. L. Andrew, *Adv. Mater. Technol.* **2019**, *4*, 1800615; g) H. M. Elmoughni, A. K. Menon, R. M. W. Wolfe, S. K. Yee, *Adv. Mater. Technol.* **2019**, *4*, 1800708.

[9] a) C. Dun, C. A. Hewitt, H. Huang, D. S. Montgomery, J. Xu, D. L. Carroll, *Phys. Chem. Chem. Phys.* **2015**, *17*, 8591; b) X. Hu, K. Zhang, J. Zhang, S. Wang, Y. Qiu, *ACS Appl. Energy Mater.* **2018**, *1*, 4883; c) Y. Wang, S. M. Zhang, Y. Deng, *J. Mater. Chem. A* **2016**, *4*, 3554; d) Y. Wang, G. Liu, M. Sheng, C. Yu, Y. Deng, *J. Mater. Chem. A* **2019**, *7*, 1718; e) E. J. Bae, Y. H. Kang, C. Lee, S. Y. Cho, *J. Mater. Chem. A* **2017**, *5*, 17867.

[10] a) D. Madan, Z. Wang, A. Chen, P. K. Wright, J. W. Evans, *ACS Appl. Mater. Interfaces* **2013**, *5*, 11872; b) C. Ou, A. L. Sangle, A. Datta, Q. Jing, T. Busolo, T. Chalklen, V. Narayan, S. Kar-Narayan, *ACS Appl. Mater. Interfaces* **2018**, *10*, 19580; c) C. Zhou, C. Dun, Q. Wang, K. Wang, Z. Shi, D. L. Carroll, G. Liu, G. Qiao, *ACS Appl. Mater. Interfaces* **2015**, *7*, 21015; d) X. Zhao, W. Han, C. Zhao, S. Wang, F. Kong, X. Ji, Z. Li, X. Shen, *ACS Appl. Mater. Interfaces* **2019**, *11*, 10301; e) R. Mulla, M. K. Rabinal, *ACS Comb. Sci.* **2016**, *18*, 177; f) A. L. Pires, I. F. Cruz, J. Silva, G. N. P. Oliveira, S. Ferreira-Teixeira, A. M. L. Lopes, J. P. Araújo, J. Fonseca, C. Pereira, A. M. Pereira, *ACS Appl. Mater. Interfaces* **2019**, *11*, 8969; g) C. Sun, A. H. Goharpey, A. Rai, T. Zhang, D.-K. Ko, *ACS Appl. Mater. Interfaces* **2016**, *8*, 22182; h) T. Zhang, K. Li, C. Li, S. Ma, H. H. Hng, L. Wei, *Adv. Electron. Mater.* **2017**, *3*, 1600554; i) X. Zeng, C. Yan, L. Ren, T. Zhang, F. Zhou, X. Liang, N. Wang, R. Sun, J.-B. Xu, C.-P. Wong, *Adv. Electron. Mater.* **2019**, *5*, 1800612; j) T. Sugahara, Y. Ekubaru, N. V. Nong, N. Kagami, K. Ohata, L. T. Hung, M. Okajima, S. Nambu, K. Suganuma, *Adv. Mater. Technol.* **2019**, *4*, 1800556; k) E. Jang, A. Poosapati, D. Madan, *ACS Appl. Energy Mater.* **2018**, *1*, 1455.

[11] S. Hu, S. Zeng, X. Li, J. Jiang, W. Yang, Y. Chen, M. Li, J. Zheng, *Mater. Des.* **2020**, *188*, 108496.

[12] Y. Lin, D. Gritsenko, Q. Liu, X. Lu, J. Xu, *ACS Appl. Mater. Interfaces* **2016**, *8*, 20501.

[13] C.-W. Lin, Z. Zhao, J. Kim, J. Huang, *Sci. Rep.* **2015**, *4*, 3812.

[14] Y. Wang, H. Zhou, *Energy Environ. Sci.* **2011**, *4*, 1704.

[15] N. Kurra, D. Dutta, G. U. Kulkarni, *Phys. Chem. Chem. Phys.* **2013**, *15*, 8367.

[16] a) Y. Ryu, D. Freeman, C. Yu, *Carbon* **2011**, *49*, 4745; b) C. Cho, M. Culebras, K. L. Wallace, Y. Song, K. Holder, J.-H. Hsu, C. Yu, J. C. Grunlan, *Nano Energy* **2016**, *28*, 426; c) C. Yu, A. Murali, K. Choi, Y. Ryu, *Energy Environ. Sci.* **2012**, *5*, 9481; d) D. D. Freeman, K. Choi, C. Yu, *PLoS One* **2012**, *7*, e47822.

[17] W. Zeng, X.-M. Tao, S. Lin, C. Lee, D. Shi, K.-H. Lam, B. Huang, Q. Wang, Y. Zhao, *Nano Energy* **2018**, *54*, 163.

[18] a) J. Chen, X. Gui, Z. Wang, Z. Li, R. Xiang, K. Wang, D. Wu, X. Xia, Y. Zhou, Q. Wang, Z. Tang, L. Chen, *ACS Appl. Mater. Interfaces* **2012**, *4*, 81; b) V. Andrei, K. Bethke, K. Rademann, *Appl. Phys. Lett.* **2014**, *105*, 233902.

[19] L. B. Alemany, L. Zhang, L. Zeng, C. L. Edwards, A. R. Barron, *Chem. Mater.* **2007**, *19*, 735.

[20] a) J. Díaz, G. Paolicelli, S. Ferrer, F. Comin, *Phys. Rev. B* **1996**, *54*, 8064; b) B. Lesiak, L. Kövér, J. Tóth, J. Zemek, P. Jiricek, A. Kromka, N. Rangam, *Appl. Surf. Sci.* **2018**, *452*, 223; c) L. Stobinski, B. Lesiak, A. Malolepszy, M. Mazurkiewicz, B. Mierzwa, J. Zemek, P. Jiricek, I. Bieloshapka, *J. Electron Spectrosc. Relat. Phenom.* **2014**, *195*, 145.

[21] Y. V. Butenko, S. Krishnamurthy, A. K. Chakraborty, V. L. Kuznetsov, V. R. Dhanak, M. R. C. Hunt, L. Šiller, *Phys. Rev. B* **2005**, *71*, 075420.

[22] H. Wang, T. Maiyalagan, X. Wang, *ACS Catal.* **2012**, *2*, 781.

[23] Z. Xing, Z. Ju, Y. Zhao, J. Wan, Y. Zhu, Y. Qiang, Y. Qian, *Sci. Rep.* **2016**, *6*, 26146.

[24] M. Shim, A. Javey, N. W. Shi Kam, H. Dai, *J. Am. Chem. Soc.* **2001**, *123*, 11512.

[25] N. D. K. Tu, J. A. Lim, H. Kim, *Carbon* **2017**, *117*, 447.

[26] J. Y. Oh, J. H. Lee, S. W. Han, S. S. Chae, E. J. Bae, Y. H. Kang, W. J. Choi, S. Y. Cho, J.-O. Lee, H. K. Baik, T. I. Lee, *Energy Environ. Sci.* **2016**, *9*, 1696.

[27] K. A. Morgan, T. Tang, I. Zeimpekis, A. Ravagli, C. Craig, J. Yao, Z. Feng, D. Yarmolich, C. Barker, H. Assender, D. W. Hewak, *Sci. Rep.* **2019**, *9*, 4393.